On the calculus of smoothing kernels for seismic parameter spatial mapping: methodology and examples

David Montiel-López[1], Sergio Molina[1, 2], Juan José Galiana-Merino[3, 4], and Igor Gómez[1, 2]

[1]Multidisciplinary Institute for Environmental Studies (IMEM), University of Alicante, Crta. San Vicente del Raspeig, s/n, 03080 Alicante, Spain

[2]Department of Applied Physics, University of Alicante, Crta. San Vicente del Raspeig, s/n, 03080 Alicante, Spain

[3]University Institute of Physics Applied to Sciences and Technologies, University of Alicante, Crta. San Vicente del Raspeig, s/n, 03080 Alicante, Spain

[4]Department of Physics, Systems Engineering and Signal Theory, University of Alicante, Crta. San Vicente del Raspeig, s/n, 03080 Alicante, Spain

Correspondence: David Montiel-López (david.montlop@ua.es)

Abstract. Spatial mapping is one of the most useful methods to display information about the seismic parameters of a certain area. As in b-value times series, there is a certain arbitrariness regarding the function selected as smoothing kernel (which plays the same role as the window size in time series). We propose a new method for the calculus of the smoothing kernel as well as its parameters. Instead of using the spatial cell–event distance we study the distance between events (inter-event distance) in order to calculate the smoothing function, as this distance distribution gives information about the event distribution and the seismic sources. We examine three different scenarios: two shallow seismicity settings and one deep seismicity catalogue. The first one, Italy, allows to calibrate and showcase the method. The other two catalogues: Lorca (Spain) and the Vrancea county (Romania) are examples of different function fits and data treatment. For these two scenarios, the prior-earthquake and after-earthquake b-value maps depict tectonic stress changes related to the seismic settings (stress relief in Lorca and stress build-up zone shifting in Vrancea). This technique could enable operational earthquake forecasting (OEF) and tectonic source profiling given enough data in the time-span considered.

1 Introduction

The ultimate goal of operational earthquake forecasting (OEF) is to disseminate authoritative information using short-term time-dependent seismic hazard to help communities to prepare and manage damaging seismic emergencies. On the other hand, earthquake prediction pretends to determine the future occurrence of a given earthquake from the observable behaviour of earthquake-related parameters. Both approximations have to be given with corresponding uncertainties if the information is going to be used for further preventive action. Currently, the scientific community agrees with the hypothesis that the use of precursors has not yet provided a short-term seismic prediction framework (Uyeda and Nagao, 2018). However, in the ongoing research there is optimism on using OEF (Martinelli, 2020). Additionally, the integration of different seismic precursors in the OEF analysis might improve the reliability of the obtained results and help to improve the development of earthquake prediction systems in the future.

A seismic precursor is a phenomenon that takes place prior to the occurrence of an earthquake. There are several precursors, classified as seismic (anomalous seismicity and micro-seismicity, swarms and fore-shocks, changes in b-value, hypocenter migration, changes in released energy and seismic waves velocities) and non-seismic (i.e. geophysical/geochemical precursors).

25 Geophysical precursors can be electromagnetic field variations, ground resistivity, telluric currents, ground deformation and crustal movements, tilt and strain and in earth tidal strain, water level changes. Meanwhile geochemical precursors are related with radon and other gases emissions, and chemical composition of underground water. These anomalous phenomena do not provide the basis for prediction of the three main parameters of an earthquake: place and time of occurrence and magnitude of the future seismic event but could forecast an increased probability of an imminent large earthquake occurrence. A more

30 detailed review of earthquake precursors can be found in Cicerone et al. (2009).

Since the 70s, when major efforts were made on promising precursors such as radon and CO_2 emissions, few advances have been achieved regarding earthquake precursors and how to develop a predictive model. However, on short time scales, less than a few months, earthquake sequences show a high degree of clustering in space and time. The probability of triggering increases with the initial shock's magnitude and decays with elapsed time according to simple scaling laws. The first generation

35 of models used for short-term clustering of earthquakes are the Omori law (Omori, 1984), Omori-Utsu law -also known as Modified-Omori (Utsu, 1961, 1969)-, and then Reasenberg and Jones (1989), in chronological order.

The Gutenberg-Richter (Equation 1, G-R from now on) empiric Law (Gutenberg and Ritcher, 1956) has been and still is one of the most used mathematical models that aims to explain the magnitude-frequency earthquake distribution based on the observations compiled in the catalogues. The main reason for its popularity is its simple formulation, which in turn enables a

40 more straightforward computer-based data process.

$$\log_{10} N_{M \geq m}(m) = a - b \cdot m \tag{1}$$

Where a is the earthquake productivity for the area; b is related to the ratio between high magnitude and low magnitude earthquakes and $N_{M \geq m}$ is the number of earthquakes with magnitudes M greater than a threshold magnitude, m.

The main constraint of this empiric law is that the catalogue must describe a homogeneous Poisson point process, that is,

45 the process is random and the average number of events that occur per time unit, λ, is constant (no matter the length of the considered interval).

Recent studies have shown the importance of the so-called b-value regarding seismic risk assessment by relating its low values (depending on the tectonic regime and the area) to tectonic stress build-up (Gulia and Wiemer, 2010) Moreover, the conclusions of this work agree with tests conducted in laboratory scale (Wiemer and Schorlemmer, 2007). Finally, Galiana-

50 Merino et al. (2022) proved the viability of using radon measurements to estimate the daily seismic activity rate. Then, time-dependent seismic hazard or risk can be computed using seismic and non-seismic information (e.g., radon) to provide useful results for OEF.

All the previous studies rely on an accurate estimation of the spatiotemporal variations of the b-value. They will be discussed in the next part.

1.1 Temporal variations of the b-value

The temporal distribution of earthquakes for a given tectonic region is usually used to evaluate the change of the b-value before and after the occurrence of the main event in a certain area. The ability to monitor the seismic activity and the increase in the detection and characterization of the earthquakes in a certain area or fault is what makes this technique interesting.

The number of events used for the b-value estimation is a parameter that distinguishes two different methods: the rolling window method (RW) and the weighted likelihood method (WL).

RW has been used for a long time and can be seen in different studies (e.g., Gulia et al., 2016; Gulia and Wiemer, 2019; Smith, 1981). This method relies on the definition of an event window (considering a fixed number of events or for a certain period) for a stable b-value calculus. It is easy to implement and only requires a quick inspection of the temporal event distribution to determine the event window size.

Often, the size of this window is chosen arbitrarily which means there may be a better choice or that the results may be not accurate in some windows. DeSalvio and Rudolph (2021) pointed out in their work that the Traffic Light System developed by Gulia and Wiemer (2019) for forecasting earthquakes with fore-shocks higher than $M_w \geq 6$ should be evaluated with parameters obtained by optimization in the parameter space rather than handpicked values.

On the other hand, WL was introduced by Tormann et al. (2014) in order to eliminate the event window size choice (generally arbitrary) and has been used recently by Taroni et al. (2021a). It uses a time-decaying exponential weight function, which parameter has been optimized by means of an exponential likelihood function. The main advantage of this method is that it avoids any arbitrary choice of parameters, so using different datasets with the same algorithm is enabled without previous event distribution studies.

1.2 Spatial distribution of the b-value

The computation and mapping of the spatial distribution of the b-value is a useful tool regarding information showcasing. Depending on the data and the level of detail it can help describing structures such as faults or tectonic stress build up zones (García-Hernández et al., 2021).

There are several examples of b-value spatial mapping due to shallow seismicity. Tormann et al. (2014) mapped the details of several faults from California (U.S.) and their tectonic stress distribution by developing a distance-dependent sampling method. Taroni and Akinci (2021) included foreshocks and aftershocks in the computations by means of a weight function, so the catalogue does not need to be declustered, although all the existing seismic series have to be identified. Additionally, depth profiles of the b-value spatial distribution are also useful for analysing the tectonic behaviour responsible of the intermediate and deep seismicity. Amongst others, Wiemer and Wyss (2002) computed the b-value in-depth changes to understand the seismic activity due to volcano related seismicity. More recently, Batte and Rümpker (2019) used this technique to analyse the shallow seismicity and relate the high b-values to heat flow in a rift environment. Chiba (2022) mapped the b-value distribution for the area from North Okinawa to Southern Kyushu Island (Japan), a region with a complex and rich tectonic setting, so the zones with more seismogenic potential are showcased.

When computing the spatial distribution of the b-value, different smoothing kernels are used to weight down the events depending on the distance from the spatial grid cell in which the b-value is calculated. The comparison between the event windows in the time series and the smoothing kernels can be made as they play the same role in the b-value calculus.

Another issue that has to be addressed is the method chosen for the estimation of the cut-off magnitude calculus. Recent work (Zhou et al., 2018) has shown that the characteristics of the seismic catalogue determine which algorithm suits better the cut-off or threshold magnitude calculus which is needed to calculate the b-value according to Aki (1965).

Following the argument from the previous part regarding window sizes, the smoothing kernel should not be chosen arbitrarily, it will be necessary to find a way to correlate the event distribution with the smoothing kernel. Therefore, we propose to correlate the epicentre spatial distribution of the events in the catalogues to determine the smoothing kernel to be used in the seismic parameter spatial mapping. The function that best describes the spatial distribution of the events of the catalogue will be also the best to approach neighbouring events when calculating the b-value in a given spatial cell.

1.2.1 Smoothing kernels in spatial mapping

According to the definition of the weight functions, the parameter σ (Brunsdon et al., 2002), regarded as a bandwidth, determines the focus or level of detail, so the higher this parameter, the slower this smoothing kernel function decays over space and vice versa. This means that the lower σ values the higher level of detail.

Recently, Taroni et al. (2021b) refined Tormann et al. (2014) methodology to plot the spatial distribution of the b-value in Italy, and although there exists controversy in the conclusions (Gulia et al., 2022), our main interest is the methodology and the event catalogue. They employed the σ value calculated by Murru et al. (2016), by means of the maximization of the likelihood of the seismicity contained in half the CPTI15 catalogue and obtained a smoothing parameter of $30\,\mathrm{km}$ for central Italy.

One of the main weaknesses of the non-Epidemic Type Aftershock Sequence (ETAS) b-value spatial mapping current methodologies is the fact that there is no clear justification on the use of the smoothing kernel function based on the event-spatial grid cell distance for regional b-value mapping. Both the spatial grid cell size and resolution are arbitrary and do not provide information of the seismic sources of the zone, as the grid's extent only purpose is to contain all the events of the catalogue. Although the influence of the grid choice can be minimized as pointed out by Tormann et al. (2014), this distance distribution does not relate to each event's source. We introduce a methodology that relies on the analysis of the inter-event distance distribution for the fit of the smoothing kernel function and its parameters in order to optimize the resolution of b-value mapping.

2 Methodology

In order to obtain the smoothing kernel function and its parameters for a given seismic catalogue, we will follow the next steps.

First, it is necessary to study both the inter-event distance and the spatial cell-event distance distribution. These quantities can be calculated once the Euclidean coordinates are obtained for each event and the spatial cell of the grid (Equation 2):

$$d = \sqrt{(x_1 - x_2)^2 + (y_1 - y_2)^2} \qquad (2)$$

120 Where d is the Euclidean distance, x is the abscissa and y is the ordinate of each point (event or centre of the spatial cell).

The main problem regarding this step arises when the catalogues are extensive. The number of events can increase the memory requirements for the inter-event distance calculus, as for each event it will be necessary to calculate as many distances as events exist in the catalogue. For example, if the catalogue has 50000 events it will be necessary to allocate enough memory to store a 50000 by 50000 float-type array. This can also happen when calculating the spatial cell-event distance distribution 125 depending on the area's size or the spatial cell resolution.

There are several ways to work around this situation. If the area does not display many seismic clusters, i.e., the distribution of the events can be approximated as a random one, then a set of random events in the catalogue can be used to calculate the distance distribution instead of the full catalogue. For this condition to be fulfilled, the area should be sized so no tectonic features (around which the events may cluster) have influence on the seismic record. Another option is to split the catalogue 130 into several parts when the previous condition cannot be fulfilled. Tormann et al. (2014) proposed the introduction of a cut-off distance for the calculus of the spatial cell-event distance-based weight function values. According to their work, the events further than 7.5 km have no influence on the outcome so they can be ignored. To avoid the loss of resolution and stability they also include a minimum number of events for each spatial cell.

In our case, the same catalogue as Taroni et al. (2021b) will be used initially and all the events of the catalogue are considered 135 for each spatial cell b-value calculus. Instead of using a cut-off distance, the influence of the events in the b-value calculus is controlled by means of the smoothing kernel and its parameters.

Once the distances have been calculated the next step is to plot these results and analyse them. If the distance distribution can be fitted to a function, then the smoothing kernel parameters will be obtained as a result of this fit. For example, if the distance distribution is identified as a normal distribution, then σ will be calculated as the second moment of the distribution 140 (the variance).

Lastly, the weight function that will control the influence of the events on the b-value calculus should be defined. In this case, it is the result of the product of two components: the fitted function that plays the role of smoothing kernel and then a function that controls the weight of the events that belong to a seismic series following the procedures of Taroni and Akinci (2021). The final weight function can be defined as follows (Equation 3):

145 $W = W_{SK} \cdot W_{SS}$ $\qquad (3)$

Where W_{SK} is the smoothing filter and W_{SS} is the function used to add foreshocks and aftershocks into the b-value calculus.

Our methodology will be first validated using the calibration catalogue for Italy (Taroni et al., 2021b) and then we will apply it to two different seismic environments: Lorca (southeast of Spain) in the time-span around the main earthquake in the last decades (the 2011 Lorca's Earthquake M_w 5.1) and the Vrancea region (center of Romania), in a period of time also including

150   two earthquakes of M_w higher than 5. The Lorca region is dominated by shallow crustal earthquakes while the Vrancea region
       is mainly guided by intermediate and deep seismicity.

3   Results and discussion

3.1   Calibration catalogue: Italy

The Italian catalogue comprises the events from 1960 to 2019 for all Italy. It amounts up to 56309 events, which can be
155   described in terms of magnitude and depth. The depth of the events ranges from 0 to 30.0 km, so the seismicity considered
       for this area is shallow. As for the magnitudes, the minimum is 1.81 M_w and the maximum is 6.81 M_w. All the events can be
       displayed in a frequency-magnitude plot in order to examine their distribution (Figure 1).
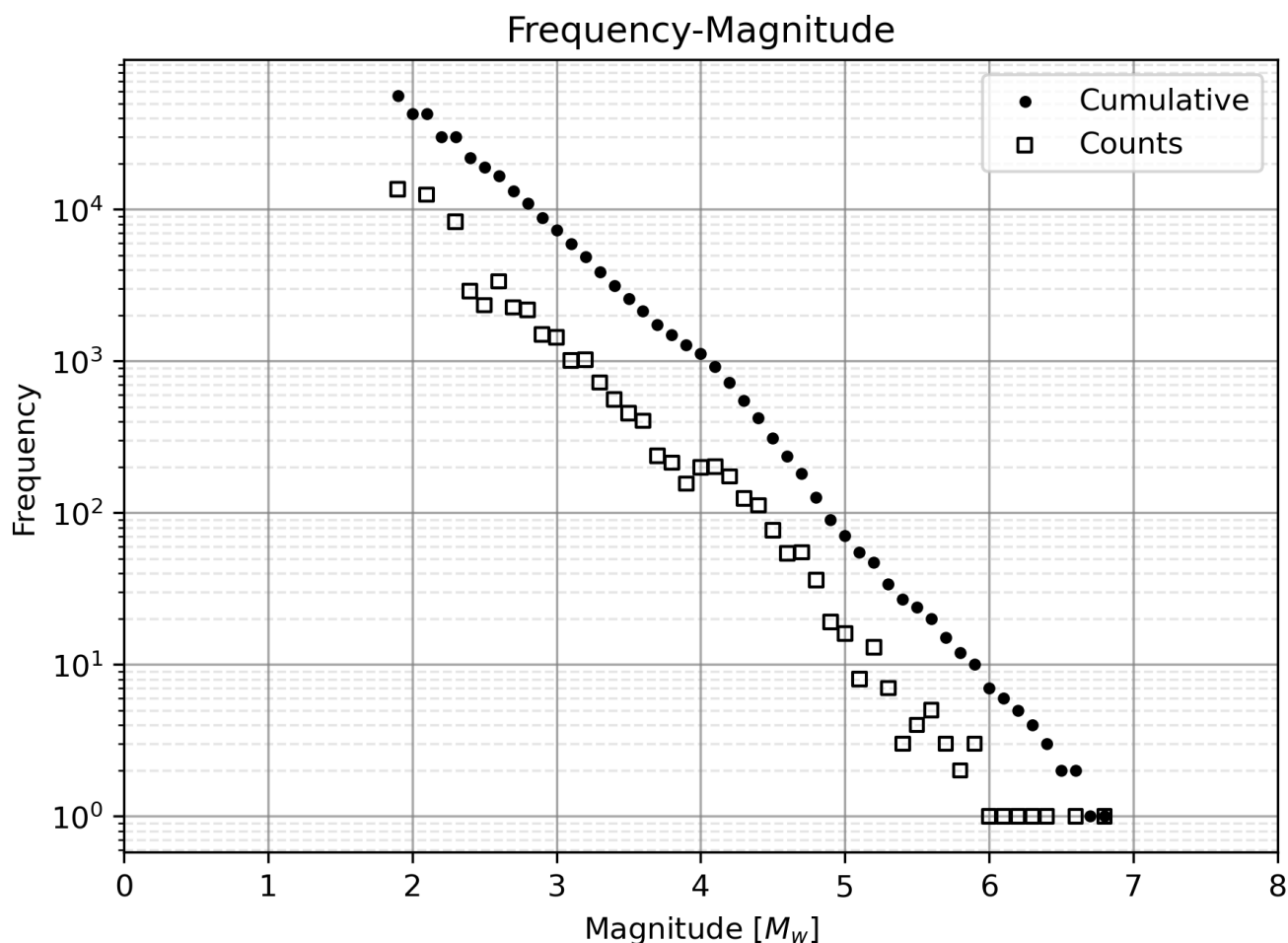
Figure 1. Frequency-magnitude plot for the Italian earthquake catalogue.

6

All the events in the catalogue have been used to plot the b-value map in order to compare the results with those obtained by Taroni et al. (2021b).

160   First, the distance between the i_{th} event with the rest of the catalogue and between the j_{th} spatial cell and the events of the catalogue ($\forall i, j$). These quantities will be called inter-event distances and spatial cell-event distance from now on.
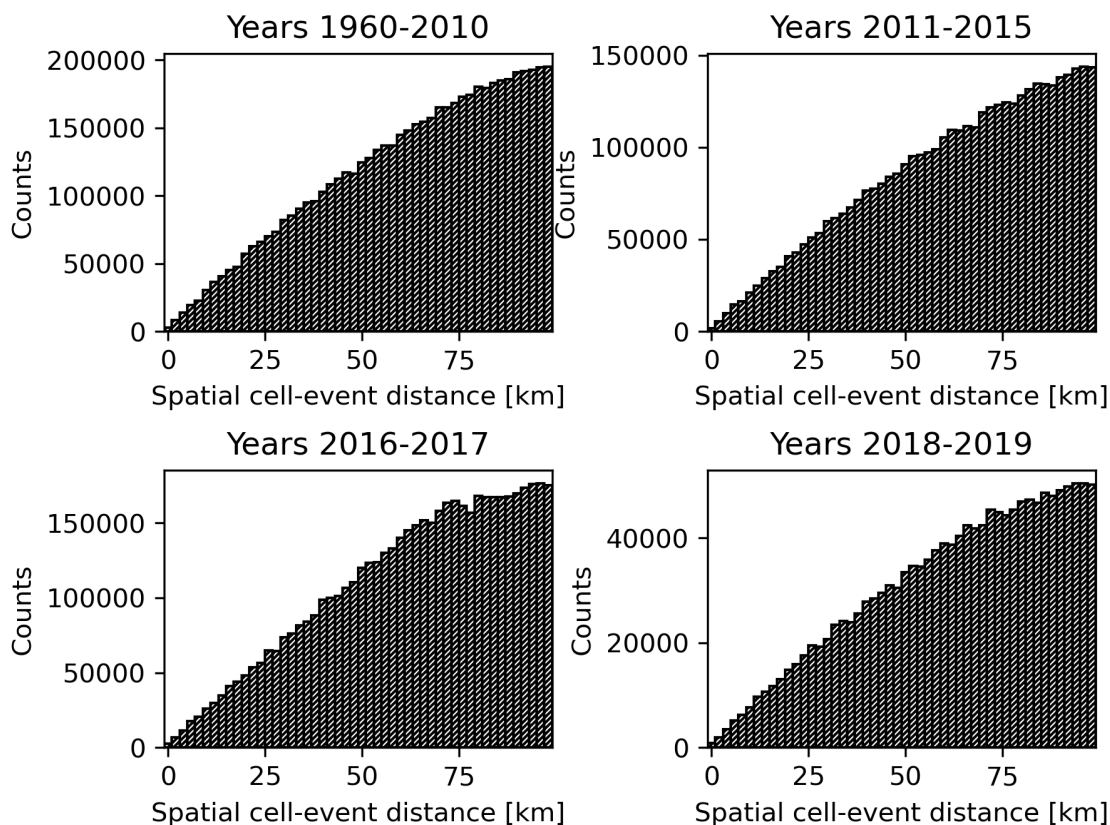

Figure 2. Histograms for spatial cell-event distances at different periods of the CPTI15 Italian earthquake catalogue.

In Figure 2, it can be seen that the spatial cell-event distance does not give useful information since the distance distribution is the same for each period as it only depends in the shape of the grid and point density. For this reason, this quantity will not be considered in further case studies.
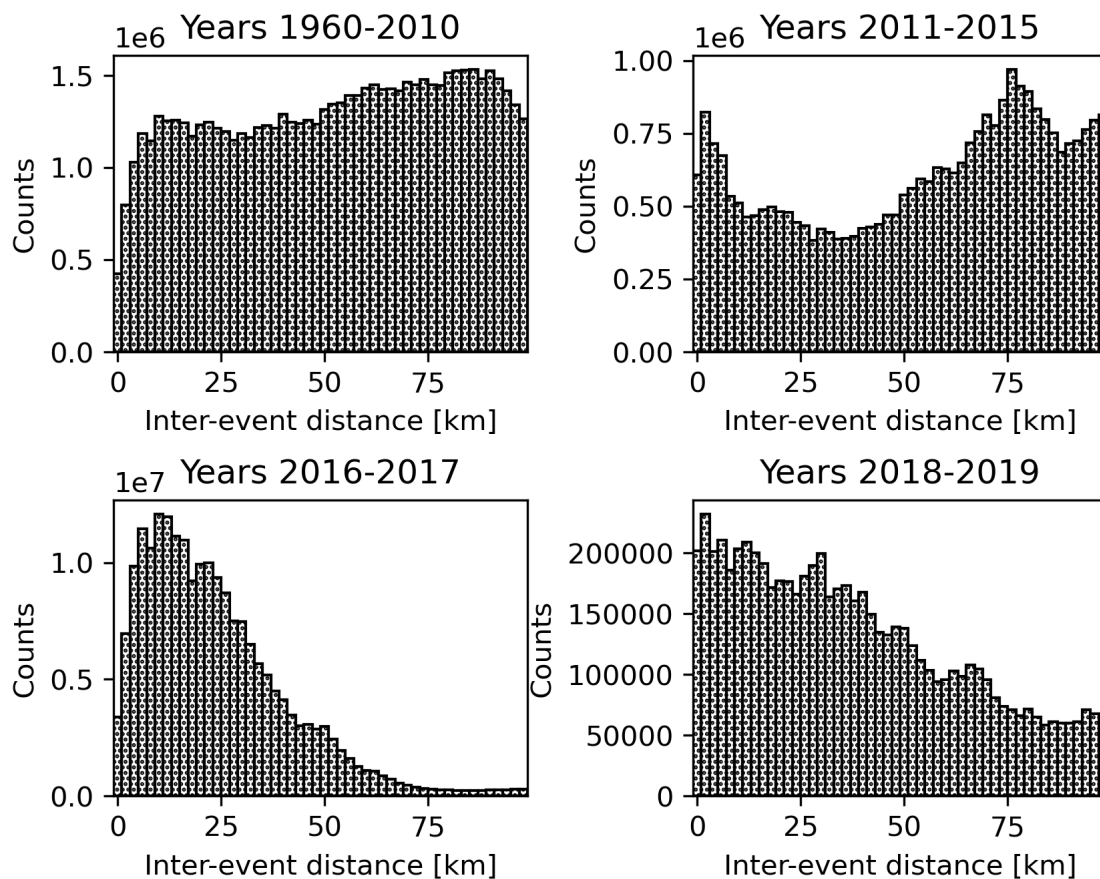
Figure 3. Histograms for the inter-event distances at different periods of the CPTI15 Italian earthquake catalogue.

165   The inter-event distance distribution shown in Figure 3 can be fitted to a different function depending on the period, but it is important to compare the number of counts in each histogram to draw further conclusions. For the period from 2016 to 2017 it can be seen that for each bin of the histogram the counts are one order of magnitude higher than for the rest of the periods. This means that this distance distribution will be representative of the catalogue except for the distances further than 50 km (for which the counts are lower and the influence of the other histograms when summed can modify the distribution).

170   All the histograms have been stacked so the inter-event distance distribution can be studied (Figure 4).
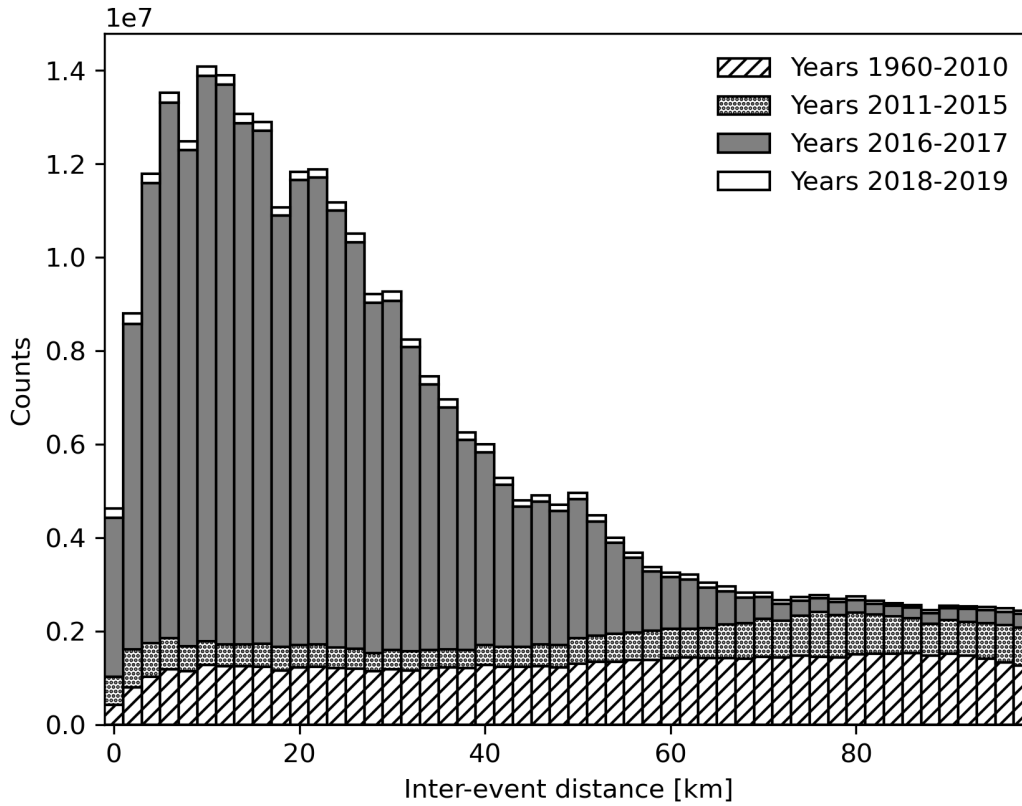
Figure 4. Stacked histogram with all the data from the inter-event distances in the Italian catalogue.

In order to obtain the smoothing kernel, two functions have been considered as fit for the data. First, the Gaussian function (Equation 4):

$$f(r) = A \cdot \exp\left(-\frac{(r - \mu)^2}{2 \cdot \sigma^2}\right) \tag{4}$$

Where A is the normalization constant, μ, is the mean value or first moment of the distribution (the maximum value of the
175   Gauss function) and σ is the standard deviation or second moment of the distribution. These will be the parameters obtained by fitting the data to this model. Although, usually, the mean value is set to zero or the data is normalized to impose a zero-mean value for simplicity (Rasmussen and Williams, 2006).

An exponential-like function similar to the one used by Tormann et al. (2014) has also been considered (Equation 5):

$$f(r) = d \cdot r \cdot \exp\left(-r \cdot c\right) \tag{5}$$

180   Where r is the distance and c and d are both real parameters that will be adjusted using the test data shown in Figure 4. For this function to be fitted, the count distribution has been normalized so the parameters can be used for the weight function calculus.
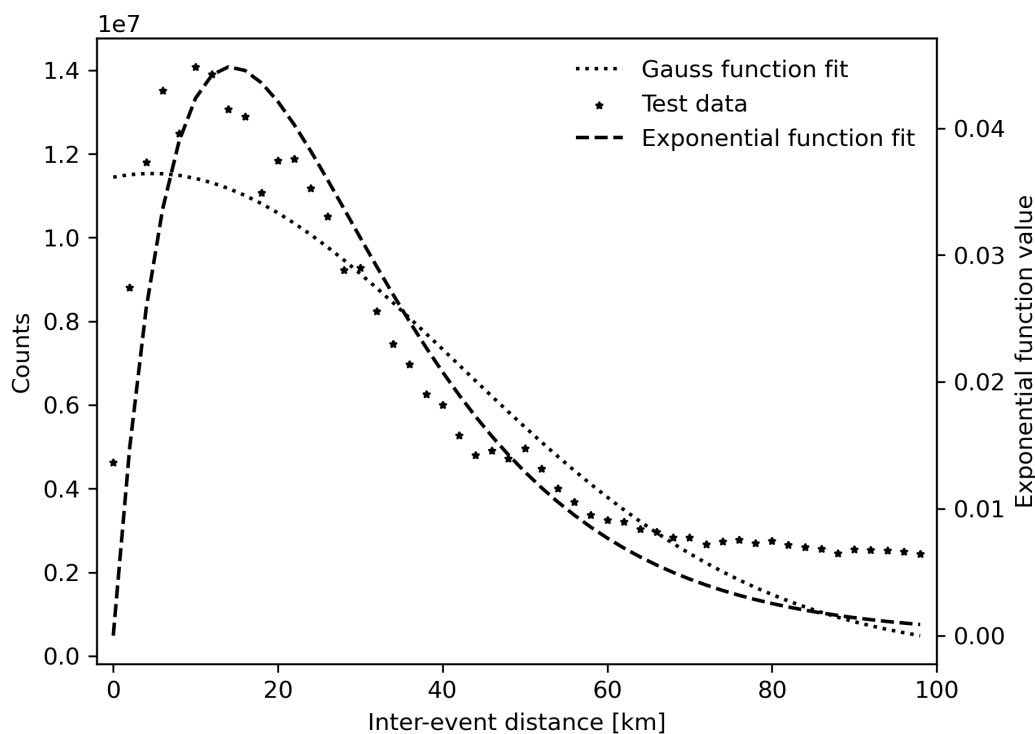

Figure 5. Comparison between both the Gaussian function fit and exponential-like function fit for the stacked counts in the inter-event distance distribution for the Italian catalogue.

The exponential-like function is a better fit for the inter-event distance distribution as it can be seen in Figure 5. The parameters of both the Gaussian and exponential function are shown in Table 1.

Table 1. Parameters obtained by fitting the Gaussian and exponential function to the counts in the inter-event distance distribution for the Italian catalogue.

Function	σ / c	μ / d	R^2	S
Gauss	40 ± 5	5 ± 7	0.839	1,688,051
Exponential	0.070 ± 0.003	0.009 ± 0.001	0.918	0.006

185   The next step is the comparison of the results obtained by using the exponential-like kernel with those presented by Taroni et al. (2021b).
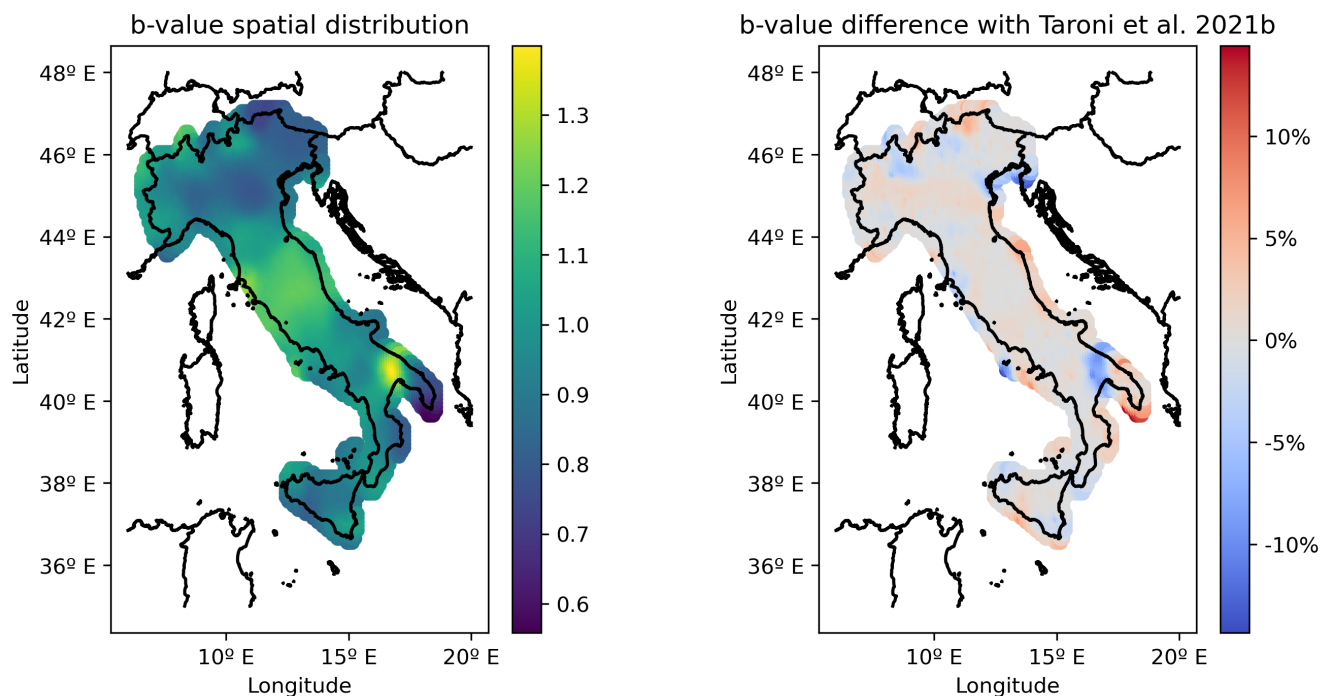

Figure 6. Spatial distribution of the b-values obtained in this work (left) and the percentage change of these with the b-values from Taroni et al. (2021b) (right). 56309 events used in each spatial cell.

The difference between the two spatial maps is lower than 2 % in most of the country except for border areas in which the difference can rise up to a 15 % as it can be seen in Figure 6. This can be due to less data being available for the b-value calculus (border effect).

190   Once the proposed methodology to obtain the smoothing kernel value in order to compute the b-value spatial distribution has been tested, it will be applied to two different case studies.

3.2   Case study: Lorca and Vrancea region

3.2.1   Lorca's Area (Spain)

For the area of Lorca, we select the following region centered around the epicentre of Lorca's earthquake that happened the
195   11th May 2011, 16:47 UTC. This event has been extensively studied. For instance, Martinez-Diaz et al. (2012) studied the rupture of the Alhama de Murcia fault and calculated the stress build-up and release using different fault models by means of interferometry data to account for the co-seismic deformation. González et al. (2012) studied the relationship between the

crustal stress changes and the co-seismic slip distribution. Frontera et al. (2012) performed a comparison of the deformation by means of data and numerical models. More information about Lorca's earthquake can be found in the special issue of the
200   Bulletin of Earthquake Engineering (Álvarez and Oterino, 2014).

     In order to apply the proposed methodology, the Spanish earthquake catalogue (can be found in: https://www.ign.es/web/ign/portal/sis-catalogo-terremotos) was filtered selecting the events in a 40 km radius circumference centered at Lorca's earthquake epicenter. Events have been selected from year 2000 to 2021 to have enough data to plot the b-value (Figure 7). This catalogue has a total of 2962 events with magnitudes between 0.8 M_w and 5.0 M_w and depths that range from 0 to 32.0 km. The
205   seismicity can be described as low to moderate in size and shallow.
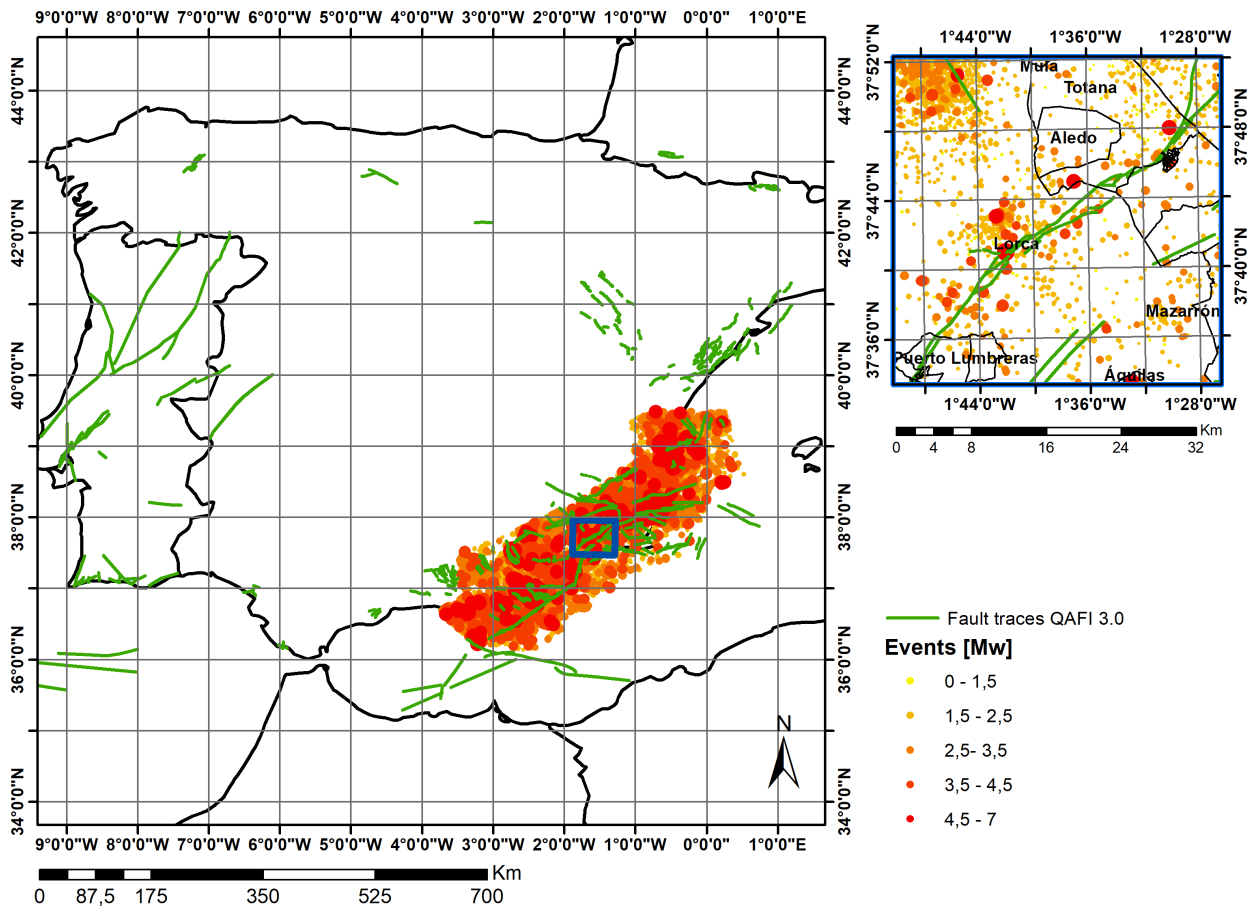

Figure 7. Southeastern Spain's seismic catalogue, zoom over Lorca's area (left) and fault traces in green from QAFI 3.0 (García Mayordomo et al., 2012).

The catalogue has been divided in two parts: a pre-series period (from 2000 to 2010) and post-series period (from 2012 to 2020) so the b-value maps can be studied. Following the procedure described in the former example, the inter-event distributions have been plotted and the two functions presented before have been fitted in order to obtain the smoothing kernel function and its parameters.
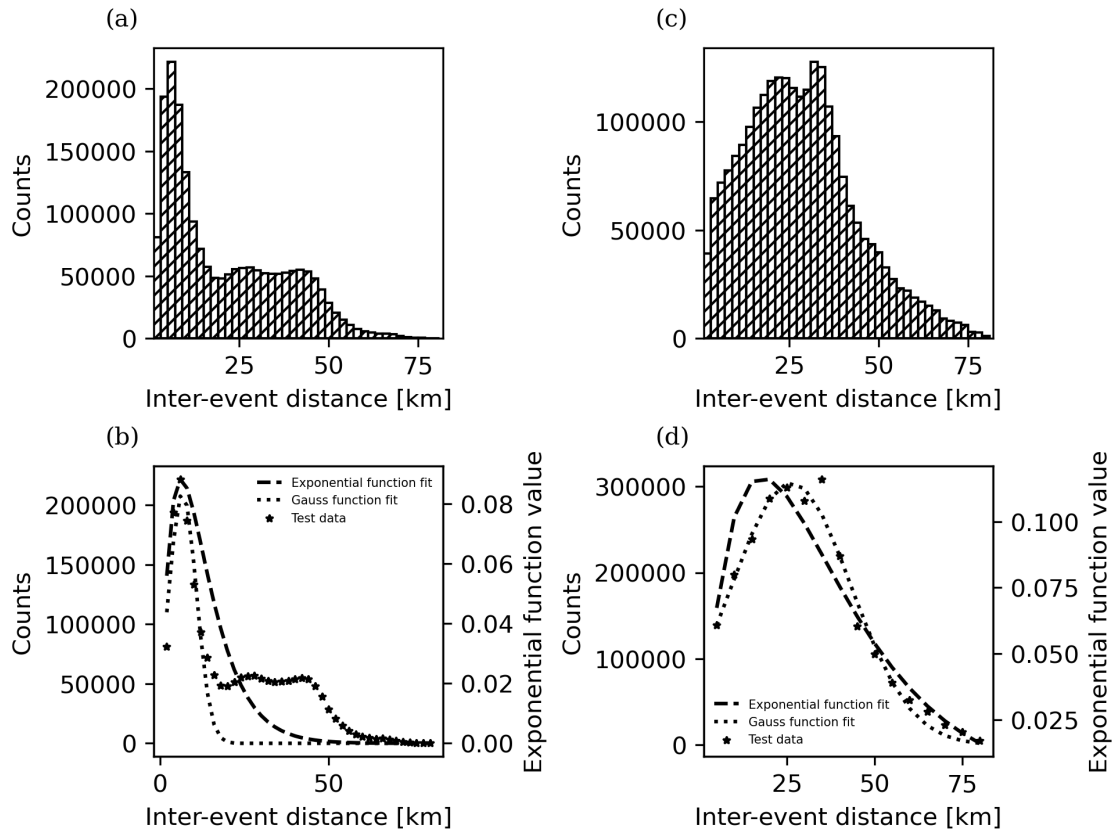

Figure 8. (a) Inter-event distance distribution for events from 2000 to 2010. (b) Functions fit of the inter-event distance distribution counts up to 14 km distance for the data from 2000 to 2010. (c) Inter-event distance distribution (down) for events from 2012 to 2020. (d) Functions fit of the inter-event distance distribution counts up to 80 km distance for the data from 2012 to 2020.

Then, Figure 8 represents the inter-event distance distribution. As it can be seen, there is no clear distribution for the $0 - 100$ km interval in the first period, a). However, the extension of the area allows considering only the first 14 km of the distance distribution. The Gaussian function has been fitted in b) with this constrain. As for the exponential function all the data has been used. For the second period (2012-2020), the distance distribution in c) shows a more clear tendency, for this reason the functions that have been fitted in d) use all the available date. The parameters obtained are represented in Table 2.

Table 2. Parameters obtained by fitting the Gaussian and exponential function to the counts in the inter-event distance distribution for Lorca's area catalogue. Last two columns show the R^2 of the model and the standard error of the regression (S).

Period [yrs]	σ	μ	c	d	Gaussian		Exponential	
					R^2	S	R^2	S
2000-2010	4 ± 1	6.7 ± 0.4	0.16 ± 0.01	0.04 ± 0.01	0.872	27034	0.784	0.015
2012-2020	16 ± 1	26 ± 1	0.056 ± 0.004	0.018 ± 0.002	0.982	16337	0.893	0.018

215   It can be seen in both the Figure 8 and the Table 2 that the Gaussian function is a better fit for the inter-event distance distribution. Then, using this smoothing kernel, the b-value distribution for both periods is plotted:
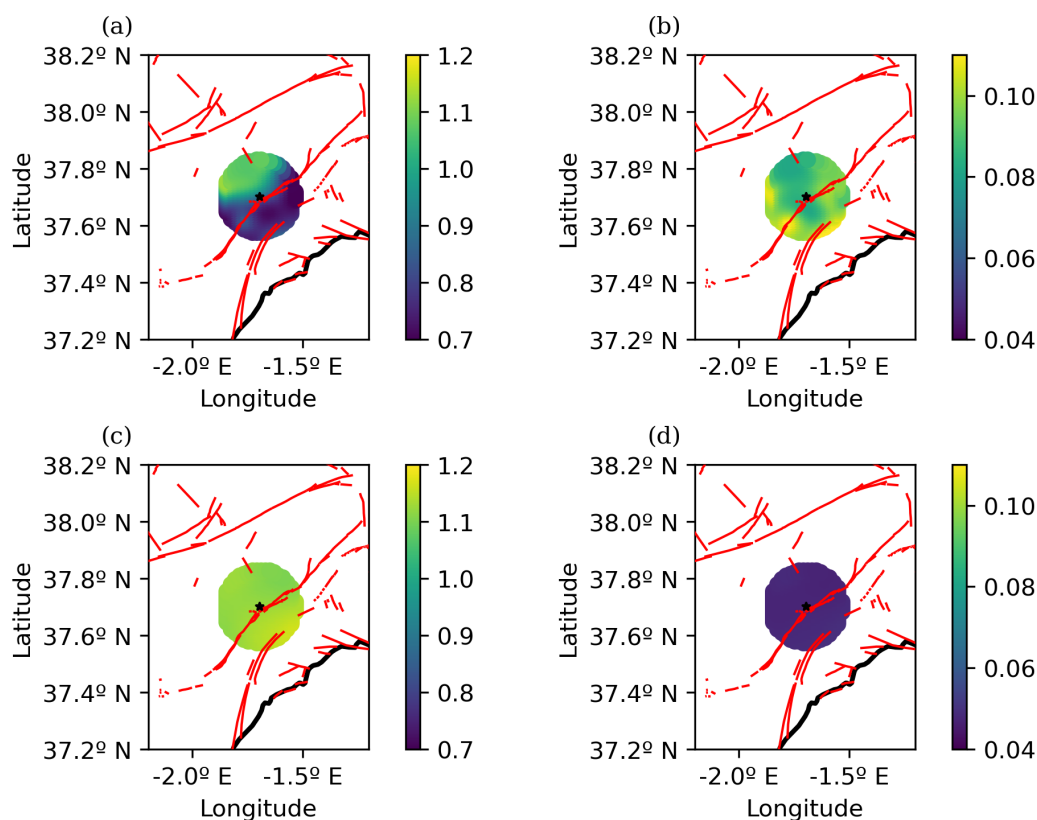

Figure 9. (a) Spatial distribution of the b-value and (b) its uncertainty in Lorca's area using data from 2000 to 2010 and the σ and μ values obtained before. 981 events have been used in each spatial cell. (c) Spatial distribution of the b-value and (d) its uncertainty in Lorca's area using data from 2012 to 2020 using the σ and μ values obtained in the previous step. 824 events have been used in each spatial cell. The red lines are the fault traces from QAFI 3.0 (García Mayordomo et al., 2012) and the black star marker shows the location of Lorca's earthquake epicenter.

Figure 9a shows that the b-values in the proximity to the fault responsible of the Lorca earthquake (in the center of the circle) are lower than the tectonic zone's mean value (b = 1.03, García Mayordomo et al., 2012). As this part of the catalogue comprises ten years before the Lorca's earthquake, the b-value spatial distribution calculated shows a zone of increased tectonic stress in the NE and SW parts of the fault, before the main Lorca's series event.

In Figure 9c it can be seen that the b-values are higher than the average value cited before. This could imply that part of the tectonic stress build-up has been released by means of the earthquakes of Lorca's series.

3.2.2 Vrancea region (Romania)

The Vrancea region, 135 km apart from Romania's capital, Bucharest, is one of the zones with highest seismic activity of Europe. Historical records of earthquakes show evidence of events with M_s higher than 7 (the earthquakes from 1802 and 1838) and recent events (1990's) have reached M_w higher than 6 (Zaicenco et al., 2008).

It is noteworthy to highlight that all strong earthquakes registered have occurred at depths greater than 60 km, which have become the focus of research for this zone. The up-to-date catalogue of Romania can be found in the following adress: http://www.infp.ro/index.php?i=romplus.
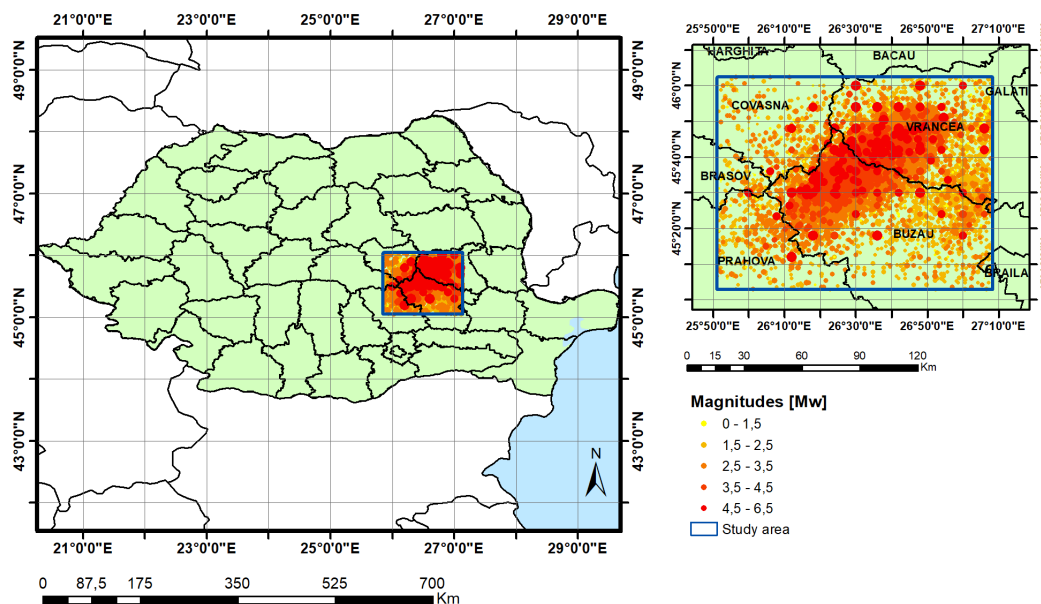

Figure 10. Plot of the catalogue from 2016 to 2020 in the Vrancea region (Romania). Romanian province shapefile obtained from WorldBank: Counties of Romania (National Agency of Cadastre and Land Registration).

230   Taking into consideration that the region has suffered three earthquakes with M_w 5.5 in the last decade, then we have chosen the events from 2016 to 2020 in the Vrancea region. The b-value mapping area is comprised inside the blue frame in Figure 10, in which all the events of the catalogue are shown.

The catalogue contains 12390 events with magnitude ranging from M_w 1 to M_w 7.7. 32 % have shallow depth, 21 % have intermediate depth and 47 % have deep depth. As we can see the most of them (68 %) are intermediate and deep seismicity.

235   The events can be plotted in the frequency-magnitude graph depending on their depth. In this case deep seismicity accounts for intermediate and deep events (> 50 km depth) and shallow seismicity for those with depth lesser than 50 km.
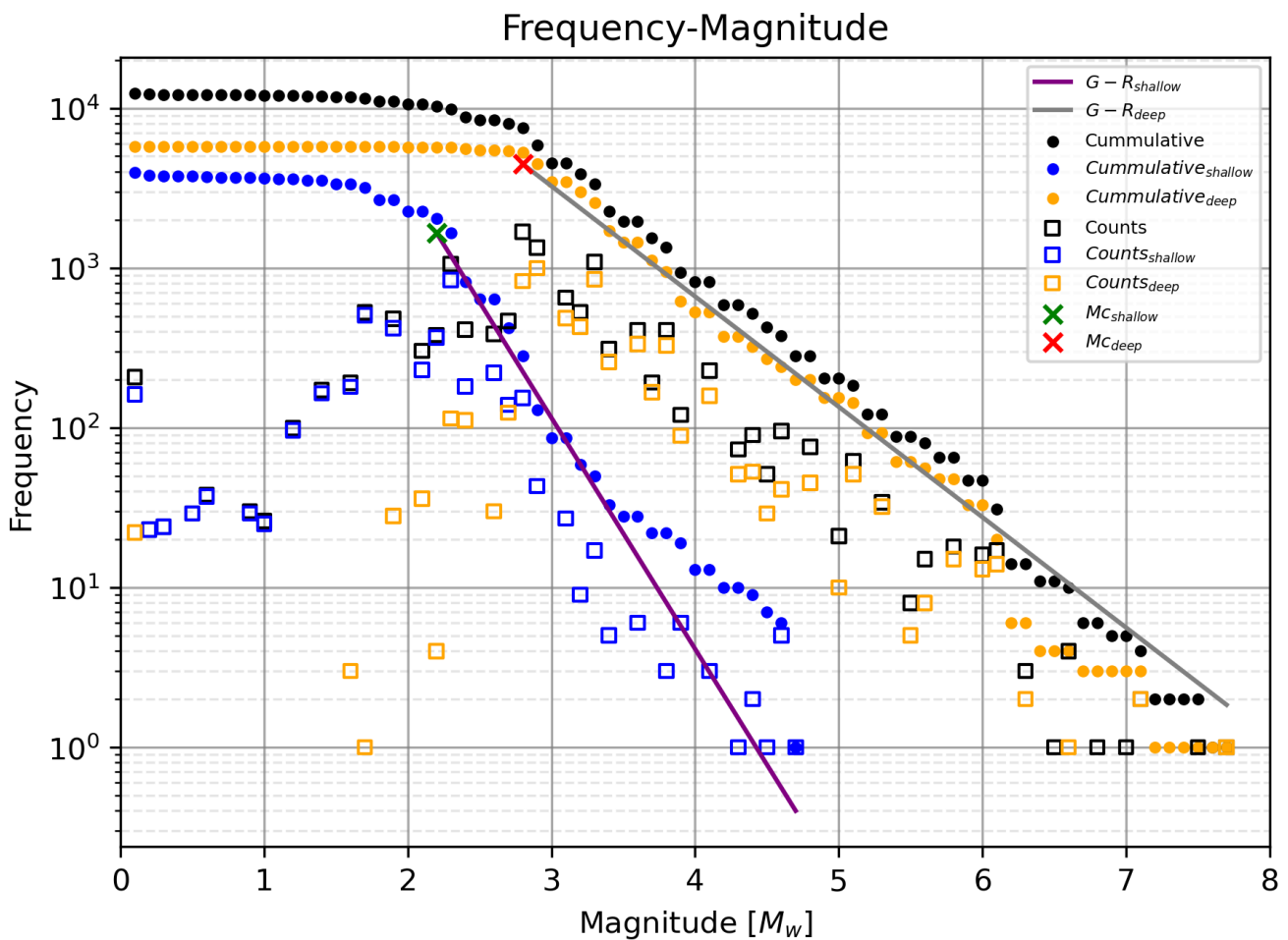

Figure 11. Frequency-Magnitude plot for the full catalogue (black), shallow events (< 50 km depth) and deep events (> 50 km). The counts are shown with void square markers and the cumulative representation in dots. The G-R law has been fitted for both the deep events and shallow events catalogue.

Figure 11 represents the magnitude-frequency distribution of the earthquakes at different depths and the tendency of the G-R law. The different slopes indicate that separate catalogues should have been used to compute the spatial b-value distribution for each depth range. As the moderate to large earthquakes have a depth greater than 50 km, then we will consider only
240   intermediate and deep seismicity for the study.

In this zone two major earthquakes occurred: the September 24th of September 2016, 23:11 UTC and the 28th of October 2018, 00:38 UTC . The catalogue will be split in two parts: from 2000 to 2015, and from 2017 to 2018 (before the earthquake happened) in order to compare the b-value spatial distribution. The first step is to calculate the event distance distribution as in the previous cases (Figure 12).
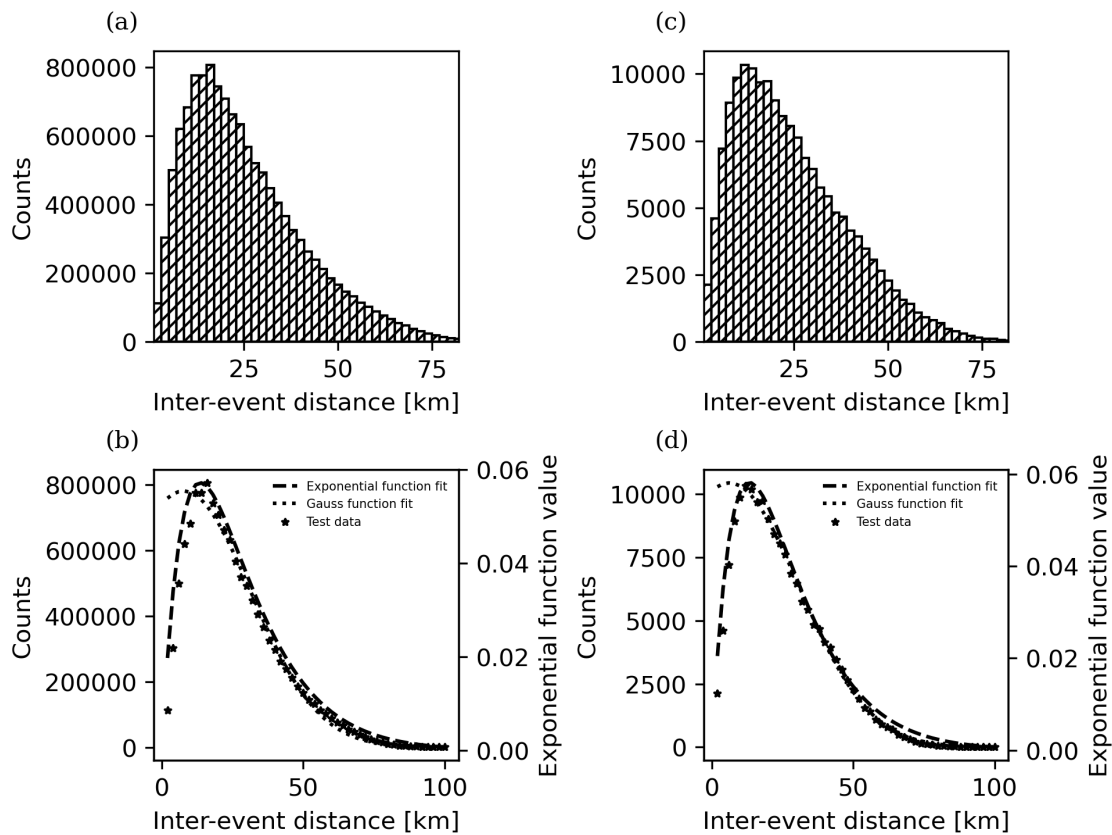

Figure 12. (a) Inter-event distance distribution for events from 2000 to 2015. (b) Functions fit for the inter-event distance distribution for events from 2000 to 2015. (c) Inter-event distance distribution for the events from 2017 to 2018. (d) Functions fit for the inter-event distance distribution for events from 2017 to 2018.

245   Both of the functions seem to fit the data, although the Gauss function overestimates the distribution in the first kilometers and the exponential function overestimates the last kilometers. The parameters obtained by means of the functions fit are provided in Table 3:

Table 3. Parameters obtained by fitting the Gaussian and exponential function to the counts in the inter-event distance distribution for the Vrancea region catalogue. Last two columns show the R^2 of the model and the standard error of the regression (S)

Period [yrs]	σ	μ	c	d	Gaussian R^2	Gaussian S	Exponential R^2	Exponential S
2000-2015	24 ± 1	8 ± 2	0.074 ± 0.001	0.0115 ± 0.0003	0.993	22767	0.985	0.003
2017-2018	25 ± 1	6 ± 1	0.075 ± 0.001	0.0120 ± 0.0003	0.998	151	0.992	0.002

Both functions will be compared. First, the Gaussian function will be used as smoothing kernel (Figure 13).
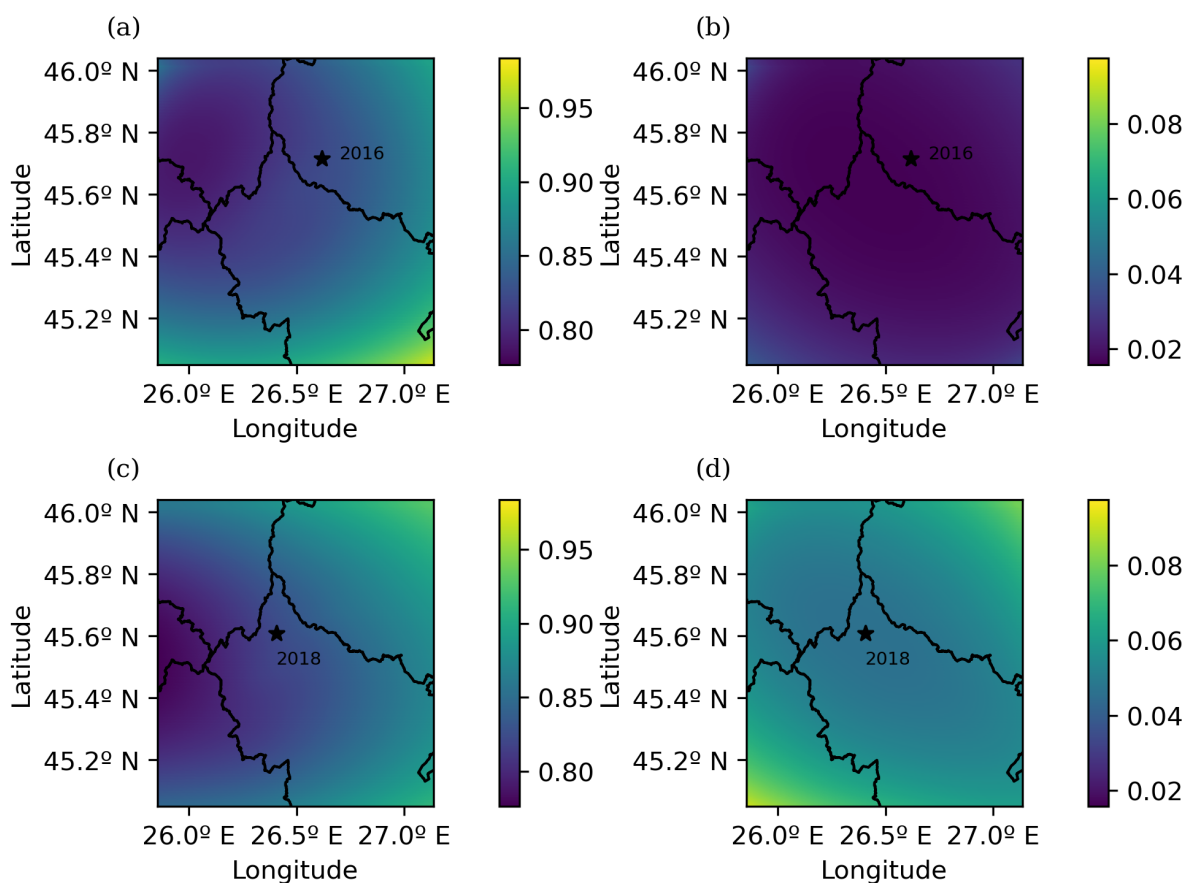

Figure 13. (a) b-value spatial mapping for the Vrancea region from 2000 to 2015 using the parameters calculated in the previous Gaussian function fit. (b) b-value uncertainty for the Vrancea region from 2000 to 2015. (c) b-value spatial mapping for the catalogue of the Vrancea region from 2017 to 2018 using the Gaussian kernel. (d) b-value uncertainty for the Vrancea region from 2017 to 2018. The black star in (a) and (b) marks the 2016 earthquake, and in (c) and (d) the 2018 earthquake.

Natural Hazards
and Earth System
Sciences
Discussions

Open Access

EGU

As it can be seen in Figure 12b and c the fit of the Gaussian function in the first 10 km is not optimal. Therefore, the
250 exponential-like function -which fits better at the first kilometers of the inter-event distance distribution- can be used in order
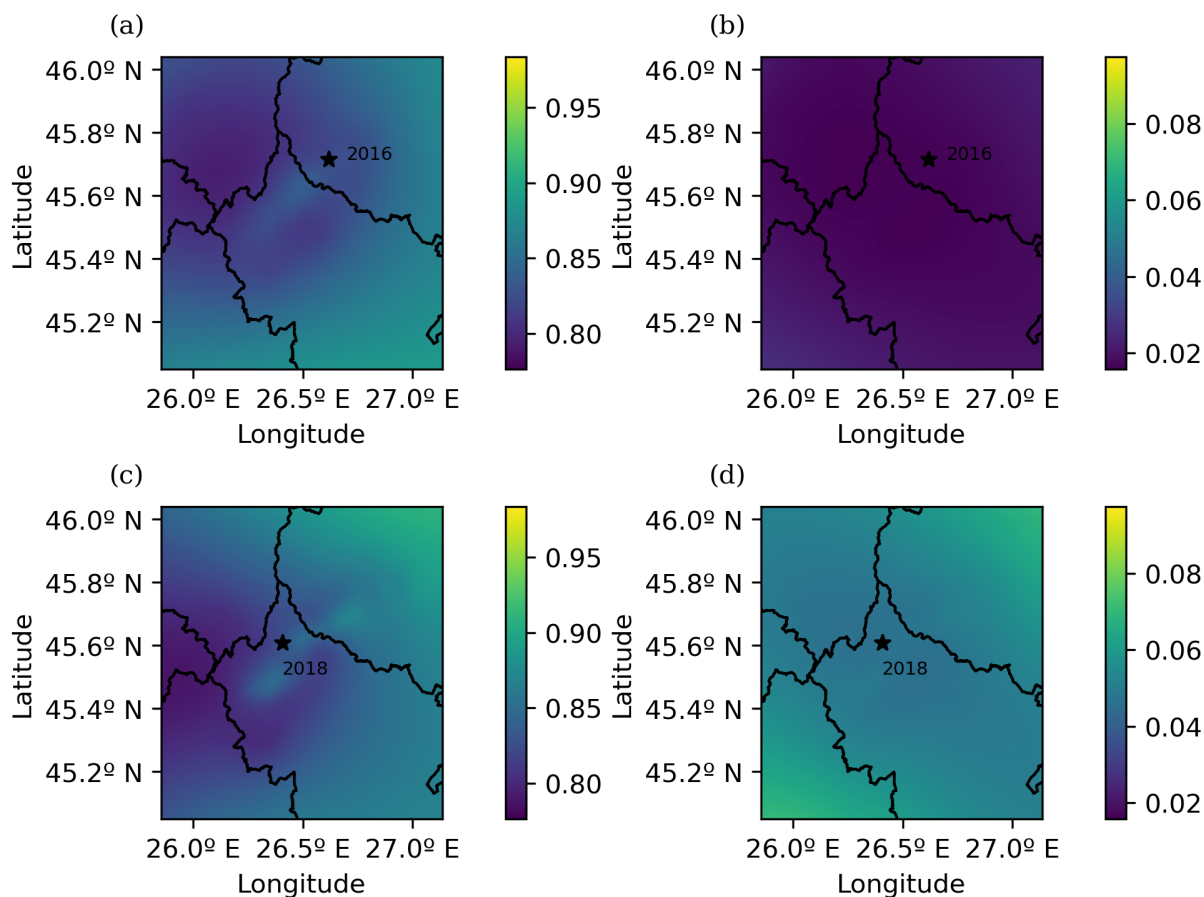to compare the results (Figure 14).

Figure 14. (a) b-value spatial mapping for the Vrancea region from 2000 to 2015 using the parameters calculated in the previous exponential function fit. (b) b-value uncertainty for the Vrancea region from 2000 to 2015. (c) b-value spatial mapping for the catalogue of the Vrancea region from 2017 to 2018 using the exponential kernel. (d) b-value uncertainty for the Vrancea region from 2017 to 2018. The black star in (a) and (b) marks the 2016 earthquake, and in (c) and (d) the 2018 earthquake.

Both b-value maps (with the different kernels) depict an increase of the b-value in zone where the the earthquake of 2016 (Figure 13c and Figure 14c) which could indicate tectonic stress relief and a slight b-value decrease towards the SW part of the area. This shifting could account to the tectonic stress build-up preceding the 2018 earthquake. The main difference 255 between the exponential function and the Gauss function when used as spatial kernels in this case is the level of detail and the b-value range (difference between the maximum and minimum value). This can be explained by examining the graphs of the exponential function fit in Figure 12b and d. The decay in the exponential function is faster than the Gauss function, so the

influence of weight function in the b-value calculus is lesser for the most remote events in the exponential function than it is in the Gaussian function.

4 Conclusions

This method for the smoothing kernel assessment and the calculus of its parameters is able to obtain results compatible with those obtained by different methods (likelihood function). Moreover, it avoids the arbitrary selection of a smoothing function by relying on a distribution fit which in also retrieves the smoothing parameters for it.

Although the spatial cell-event distance histogram has been shown for comparison purposes, it serves no use to the spatial kernel function calculus as the spatial grid is arbitrary (both in its extension and resolution) and the only constraint for this grid is to cover the entire area in which the events of the catalogue are located.

It is illustrative to use the Gaussian function as the fit for the inter-event distribution as it is a well-known function with parameters that can be easily related to the inter-event distance distribution and its characteristics. Nevertheless, other distributions can be considered as long as the function that describes them is compatible with the data as shown in the Vrancea region case study.

Another interesting topic that can be addressed is the relationship between the σ value in the case of the Gaussian function (as it is directly related with the event distribution) and the fault distribution in the study area, in case there exists one, as it could enable tectonic structure profiling.

The use of different parts of the catalogue in order to describe the b-value spatial distribution as the time passes can enable OEF as long as there is enough data for it to be stable. We used parts of the catalogue before and after a major earthquake, but it could be used to describe yearly (or even monthly depending on the zone) b-value changes.

Author contributions. DML and SM developed the original idea. JJGM and IGD helped in the development of the methodology. DML and SM performed the data curation. DML wrote the code and tested the different components. All the co-authors participated in the investigation and result interpretation. DML prepared the original draft, and SM, JJGM and IGD reviewed and edited it.

Natural Hazards
and Earth System
Sciences

Discussions

285 **References**

Aki, K.: Maximum likelihood estimate of b in the formula log N = a-bM and its confidence limits, Bull. Earthq. Res. Inst., 43, 237–239, 1965.

Álvarez, E. A. and Oterino, M. B. B.: Foreword special issue Lorca?s earthquake, Bulletin of Earthquake Engineering, 12, 1827–1829, https://doi.org/10.1007/s10518-014-9602-4, 2014.

290 Batte, A. G. and Rümpker, G.: Spatial mapping of b-value heterogeneity beneath the Rwenzori region, Albertine rift: Evidence of magmatic intrusions, Journal of Volcanology and Geothermal Res., 381, 238–245, https://doi.org/10.5414/CN108072, 2019.

Brunsdon, C., Fotheringham, A., and Charlton, M.: Geographically Weighted Summary Statistics—A Framework for Localised Exploratory Data Analysis, Computers, Environment and Urban Systems, 26, 501–524, https://doi.org/10.1016/S0198-9715(01)00009-6, 2002.

Chiba, K.: Heterogeneous b-value Distributions Measured Over an Extensive Region from the Northern Okinawa Trough to Southern Kyushu
295 Island, Japan, Pure and Applied Geophysics, 179, 1–15, https://doi.org/10.1007/s00024-022-02958-5, 2022.

Cicerone, R., Ebel, J., and Britton, J.: A systematic compilation of earthquake precursors, Tectonophysics, 476, 371–396, https://doi.org/10.1016/j.tecto.2009.06.008, 2009.

DeSalvio, N. D. and Rudolph, M. L.: A Retrospective Analysis of b-Value Changes Preceding Strong Earthquakes, Seismological Research Letters, 93, 364–375, https://doi.org/10.1785/0220210149, 2021.

300 Frontera, T., Concha, A., Blanco, P., Echeverria, A., Goula, X., Arbiol, R., Khazaradze, G., Pérez Aragüés, F., and Surinach, E.: DInSAR Coseismic Deformation of the May 2011 Mw 5.1 Lorca Earthquake (southeastern Spain), Solid Earth, 3, 111–119, https://doi.org/10.5194/se-3-111-2012, 2012.

Galiana-Merino, J. J., Molina, S., Kharazian, A., Toader, V.-E., Moldovan, I.-A., and Gómez, I.: Analysis of Radon Measurements in Relation to Daily Seismic Activity Rates in the Vrancea Region, Romania, Sensors, 22, https://doi.org/10.3390/s22114160, 2022.

305 García Mayordomo, J., Insua-Arévalo, J., Martinez-Diaz, J., Jiménez-Díaz, A., Martín Banda, R., Alfageme, M., Álvarez Gómez, J., Rodríguez-Peces, M., Perez-Lopez, R., Rodriguez-Pascua, M., Masana, E., Perea, H., Martín-González, F., Giner-Robles, J., Nemser, E., Cabral, J., Sanz de Galdeano, C., Peláez, J., Tortosa, G., and Linares, R.: The Quaternary Active Faults Database of Iberia (QAFI v.2.0), Journal of Iberian Geology, 38, 285–302, 2012.

García-Hernández, R., D'Auria, L., Barrancos, J., Padilla, G. D., and Pérez, N. M.: Multiscale Temporal and Spatial Estimation of the
310 b-Value, Seismological Research Letters, 92, 3712–3724, https://doi.org/10.1785/0220200388, 2021.

González, P., Tiampo, K., Palano, M., Cannavò, F., and Fernandez, J.: The 2011 Lorca earthquake slip distribution controlled by groundwater crustal unloading, Nature Geoscience, 5, 821–825, https://doi.org/10.1038/NGEO1610, 2012.

Gulia, L. and Wiemer, S.: The influence of tectonic regimes on the earthquake size distribution: A case study for Italy, Geophysical Research Letters, 37, 1–6, https://doi.org/10.1029/2010GL043066, 2010.

315 Gulia, L. and Wiemer, S.: Real-time discrimination of earthquake foreshocks and aftershocks, Nature, 574, 193–199, https://doi.org/10.1038/s41586-019-1606-4, 2019.

Gulia, L., Tormann, T., Wiemer, S., Herrmann, M., and Seif, S.: Short-term probabilistic earthquake risk assessment considering time-dependent b-values, Geophysical Research Letters, 43, 1100– 1108, https://doi.org/10.1002/2015GL066686, 2016.

Gulia, L., Gasperini, P., and Wiemer, S.: Comment on "High-Definition Mapping of the Gutenberg–Richter b-Value and Its Rel-
320 evance: A Case Study in Italy" by M. Taroni, J. Zhuang, and W. Marzocchi, Seismological Research Letters, 93, 1089–1094, https://doi.org/10.1785/0220210159, 2022.

Gutenberg, B. and Ritcher, C. F.: Magnitude and energy of earthquakes, Ann. Geophys., 9, 1–15, 1956.

Martinelli, G.: Previous, Current, and Future Trends in Research into Earthquake Precursors in Geofluids, Geosciences, 10, 189–209, https://doi.org/10.3390/geosciences10050189, 2020.

325   Martinez-Diaz, J., Bejar, M., Álvarez Gómez, J., Mancilla, F. d. L., Stich, D., Herrera, G., and Morales, J.: Tectonic and seismic implications of an intersegment rupture: The damaging May 11th 2011 Mw 5.2 Lorca, Spain, earthquake, Tectonophysics, 546–547, 28–37, https://doi.org/10.1016/j.tecto.2012.04.010, 2012.

Murru, M., Taroni, M., Akinci, A., and Falcone, G.: Amatrice earthquake on the seismic hazard assessment in central Italy?, Ann. Geophys., 59, 1–9, https://doi.org/10.4401/ag-7209, 2016.

330   Omori, F.: On the aftershocks of earthquakes, Journal of the College of Science, pp. 111–200, 1984.

Rasmussen, C. E. and Williams, C. K. I.: Gaussian Processes for Machine Learning, MIT Press, www.GaussianProcess.org/gpml, 2006.

Reasenberg, P. A. and Jones, L. M.: Earthquake Hazard After a Mainshock in California, Science, 243, 1173–1176, https://doi.org/10.1126/science.243.4895.1173, 1989.

Smith, W. D.: The b-value as an earthquake precursor, Nature, 289, 136–139, 1981.

335   Taroni, M. and Akinci, A.: A New Smoothed Seismicity Approach to Include Aftershocks and Foreshocks in Spatial Earthquake Forecasting: Application to the Global Mw $\geq$ 5.5 Seismicity, Applied Sciences, 11, 10 899–10 910, https://doi.org/10.3390/app112210899, 2021.

Taroni, M., Vocalelli, G., and Polis, A.: Gutenberg–Richter B-Value Time Series Forecasting: A Weighted Likelihood Approach, Forecasting, 3, 561–569, https://doi.org/10.3390/forecast3030035, 2021a.

Taroni, M., Zhuang, J., and Marzocchi, W.: High-Definition Mapping of the Gutenberg–Richter b-Value and Its Relevance: A Case Study in
340   Italy, Seismological Research Letters, 92, 3778–3784, https://doi.org/10.1785/0220210017, 2021b.

Tormann, T., Wiemer, S., and Mignan, A.: Systematic survey of high-resolution b value imaging along Californian faults: Inference on asperities, Journal of Geophysical Research: Solid Earth, 119, 2029–2054, https://doi.org/https://doi.org/10.1002/2013JB010867, 2014.

Utsu, T.: A statistical study on the occurrence of aftershocks, Geophysical magazine, 30, 521–605, 1961.

Utsu, T.: Aftershocks and earthquake statistics (1): Some parameters which characterize an Aftershock sequence and their interrelation,
345   Journal of the Faculty of Science, Hokkaido University, 3, 129–195, 1969.

Uyeda, S. and Nagao, T.: International cooperation in pre-earthquake studies: History and new directions, in: Pre-earthquakes processes. A multidisciplinary approach to earthquake prediction studies, edited by Ouzounov, D., Pulinets, S., Hattori, K., and P., T., pp. 3–6, John Wiley 'I&' Sons, 2018.

Wiemer, S. and Schorlemmer, D.: ALM: An Asperity-based Likelihood Model for California, Seismological Research Letters - SEISMOL
350   RES LETT, 78, 134–140, https://doi.org/10.1785/gssrl.78.1.134, 2007.

Wiemer, S. and Wyss, M.: Mapping spatial variability of the frequency-magnitude distribution of earthquakes, Advances in Geophysics, 45, 259–302, https://doi.org/10.1016/S0065-2687(02)80007-3, 2002.

Zaicenco, A., Craifaleanu, I.-G., and Paskaleva, I.: Harmonization of Seismic Hazard in Vrancea Zone, Springer Dordrecht, https://doi.org/10.1007/978-1-4020-9242-8, 2008.

355   Zhou, Y., Zhou, S., and Zhuang, J.: A test on methods for MC estimation based on earthquake catalog, Earth and Planetary Physics, 2, 150–162, https://doi.org/10.26464/epp2018015, 2018.